Available online at www.sciencedirect.com
ScienceDirect
International Journal of Mass Spectrometry 271 (2008) 30–35
International Journal of Mass Spectrometry
www.elsevier.com/locate/ijms

Bromine iso-electronic sequence: Lifetimes of the $4p^4 4d\ ^4D_{7/2}$ metastable level

J.P. Desclaux *

15 Chemin du Billery, Sassenage F-38360, France

Received 27 August 2007; received in revised form 18 October 2007; accepted 25 October 2007
Available online 17 November 2007

Abstract

The relativistic multiconfiguration Dirac–Fock method is applied to the calculation of the radiative decay rates from the lowest $J = 7/2$ level of the $4s^2 4p^4 d$ configuration along the Bromine iso-electronic sequence. It is shown that only a limited number of configurations is needed to include the most relevant contributions to the variation in correlation effects between this excited level and the ground $4s^2 4p^5\ ^2P_{3/2}$ state. The transition from LS to *jj* recoupling schemes along the sequence is studied and its impact on decay rates is discussed.

PACS: 31.15.Ar; 31.15.Ne; 31.25.Eb; 31.25.Jf; 31.30.Jv; 32.70.Cs

Keywords: Relativistic corrections; Correlation; Radiative decay; Lifetimes; Ions; Iso-electronic sequence

1. Introduction

Metastable levels are important in dilute plasmas because they are not depopulated by collisions but accurate values of their lifetimes are difficult to obtain both from experiment and from theory. For *ab initio* methods, how much of correlation effects have to be included is a critical issue since, excepted for few electron systems, a full correlated approach becomes intractable. On the other side, *semi empirical* methods rely on fitting some parameters to experimental results, these methods are not relevant to study trends along iso-electronic sequences. Indeed experimental results may be available near the neutral end of the sequence but the fitted values cannot be used for the high Z end of the sequence because of strong relativistic effects. To include in a consistent way both relativistic corrections, intermediate coupling and correlation contributions, we use here the multiconfiguration Dirac–Fock method with the purpose to include only the contributions significant for energies and probabilities of radiative decays. Our motivation to select the Bromine iso-electronic sequence was because of the importance of the $M2$ decay channel for the single excited KrII ion and, to our knowledge, no estimate of how this importance evolves along the sequence is known.

This paper is organized as follows: in Section 2, the method used to compute wave functions and transition probabilities is outlined. The next section contains a detailed discussion of the excited $4s^2 4p^4 4d^4 D_{7/2}$ level of KrII, for which an accurate experimental result and previous theoretical calculations are available [1], in order to assess the accuracy of the present calculations. Section 4 gives the trends along the iso-electronic sequence before we draw our conclusions.

2. Outline of the calculation method

2.1. The MCDF method

In this work, the 2007 version of the Dirac–Fock program of the author and P. Indelicato, named *mdfgme* [2] is used. Details on the Hamiltonian, angular momentum recoupling and numerical methods can be found elsewhere [3–6] below is just a brief summary for the sake of self-contained. The total energies associated with the various levels of the atomic system are given by the eigenvalues of the equation:

$$\mathcal{H}\Psi_{\Pi,J,M}(\ldots,\boldsymbol{r}_i,\ldots) = E_{\Pi,J,M}\Psi_{\Pi,J,M}(\ldots,\boldsymbol{r}_i,\ldots), \quad (1)$$

* Corresponding author.
E-mail address: jean-paul.desclaux@wanadoo.fr.

1387-3806/$ – see front matter © 2007 Elsevier B.V. All rights reserved.
doi:10.1016/j.ijms.2007.10.014

where Π is the parity, J the total angular momentum eigenvalue, and M is the eigenvalue of its projection J_z on the z axis. The Hamiltion $\mathcal{H}$ is given by

$$\mathcal{H} = \sum_i h_{\rm D}(r_i) + \sum_{i<j} V_{ij}(|\boldsymbol{r}_i - \boldsymbol{r}_j|) \tag{2}$$

with $h_{\rm D}$ the one electron Dirac operator and V_{ij} an operator representing the electron-electron interaction of order one in the fine structure constant α. The expression of V_{ij} in Coulomb gauge, and in atomic units, is

$$V_{ij} = \frac{1}{r_{ij}} \tag{3}$$

$$-\frac{\boldsymbol{\alpha}_i \cdot \boldsymbol{\alpha}_j}{r_{ij}} \tag{4}$$

$$-\frac{\boldsymbol{\alpha}_i \cdot \boldsymbol{\alpha}_j}{r_{ij}} \left[\cos\left(\frac{\omega_{ij} r_{ij}}{c}\right) - 1\right] + c^2 (\boldsymbol{\alpha}_i \cdot \boldsymbol{\nabla}_i)(\boldsymbol{\alpha}_j \cdot \boldsymbol{\nabla}_j) \frac{\cos(\omega_{ij} r_{ij}/c) - 1}{\omega_{ij}^2 r_{ij}}, \tag{5}$$

where $r_{ij} = \left|\boldsymbol{r}_i - \boldsymbol{r}_j\right|$ is the inter-electronic distance, ω_{ij} the energy of the exchanged photon between the two electrons, α_i are the Dirac matrices and c is the speed of light. It has been demonstrated that the Coulomb gauge provides energies free from spurious contributions at the ladder approximation level and must be used in many-body atomic structure calculations [7,8].

In the equations above, the term (3) is the Coulomb interaction, (4) is the Gaunt (magnetic) interaction, and the last two terms (5) stand for the retardation in the electron–electron interaction. In this expression the $\boldsymbol{\nabla}$ operators act only on r_{ij} and not on the following wave functions.

Expanding the operators of Eq. (5) in powers of $\omega_{ij} r_{ij}/c$ one obtains, at the limit $\omega_{ij} \to 0$:

$$B_{ij}^{\rm R} = \frac{\boldsymbol{\alpha}_i \cdot \boldsymbol{\alpha}_j}{2 r_{ij}} - \frac{\left(\boldsymbol{\alpha}_i \cdot \boldsymbol{r}_{ij}\right)\left(\boldsymbol{\alpha}_j \cdot \boldsymbol{r}_{ij}\right)}{2 r_{ij}^3}, \tag{6}$$

i.e., the retardation part of the Breit interaction which includes the leading retardation contribution of order $1/c^2$. The total Breit interaction is the sum of the Gaunt interaction (4) and the Breit retardation (6).

In the calculations reported here, the electron–electron interaction for the self-consistent determination of the wave functions is taken as the sum of the Coulomb and the Breit interactions. Higher orders in $1/c$, arising from the difference between operators (5) and (6) are treated here only as a first order perturbation. Radiative corrections are also added by perturbation, a detailed description of what is included in the most recent version of the *mdfgme* code can be found in [9]. All calculations are done for finite nuclei using a Fermi distribution with a thickness parameter of 2.3 fm. The nuclear radii are taken or evaluated using formulas from Ref. [10].

The MCDF method is defined by the particular choice of the total wave function to solve Eq. (1) taken as a linear combination of configuration state functions (CSF):

$$|\Psi_{\Pi,J,M}\rangle = \sum_{v=1}^{N_v} c_v |v, \Pi, J, M\rangle. \tag{7}$$

The label v stands for all other quantities (principal quantum number, degeneracy, . . .) necessary to define unambiguously the CSF besides the parity Π, the total angular momentum J and its projection J_z. Each CSF is an antisymmetric products of one-electron wave functions taken as as linear combination of Slater determinants of Dirac 4-spinors:

$$|v, \Pi, J, M\rangle = \sum_{i=1}^{N_{\rm D}^v} d_i^v \begin{vmatrix} \phi_1^i(\boldsymbol{r}_1) & \cdots & \phi_n^i(\boldsymbol{r}_1) \\ \vdots & \ddots & \vdots \\ \phi_1^i(\boldsymbol{r}_n) & \cdots & \phi_n^i(\boldsymbol{r}_n) \end{vmatrix}, \tag{8}$$

where the coefficients d_i^v are determined by requiring the CSF to be an eigenstate of J^2 and J_z and the ϕ-s are the one-electron Dirac 4-spinors:

$$\phi(r) = \begin{pmatrix} \chi_\kappa^\mu(\Omega) P(r) \\ i \chi_{-\kappa}^\mu(\Omega) Q(r) \end{pmatrix} \tag{9}$$

with χ_κ^μ a two-component spinor, and P and Q respectively the large and small component of the radial wave function. The convergence process is based on the self-consistent field process (SCF). For a given set of configurations, initial one-electron radial functions are used to build the Hamiltonian matrix and get a first set of mixing coefficients c_v. Direct and exchange potential are constructed for all orbitals, and the integro-differential equations obtained from the variational principle are solved. Then a new set of potentials is constructed and the whole process is repeated. Each time the largest variation for all radial functions has been reduced by an order of magnitude, the Hamiltonian matrix is rediagonalized, and a new cycle is started until convergence is reached.

2.2. Transition probabilities

To perform the calculations reported in the next sections, some of the specific options of *mdfgme* code are used:

- First with the option *radiative* it is enough to define the CSF for the initial and final states and, after the SCF optimization of both states, all allowed transitions probabilities for all multipoles of the electric and magnetic decay channels are computed, so that there is no need to perform separated calculations of each of the decay channels in order to find the dominant one. Transition probabilities are computed with the full operator, i.e., without low frequency approximation.
- To introduce correlation, two main options are available: either give explicitly the list of CSF to include or let the program build all single and double excitations from a reference state. In this latter case, orbitals to be excited and non-closed shells in which excitations will occur have to be specified. The second option is indeed split in more than one possibility but it is not our purpose to reproduce here part of the code's

write up, the interested reader can access it on the web site given in Ref. [2]. As an example, to include all the CSF's of the $n = 4$ shell associated with single and double excitations from the $4s^2 4p^5 J = 3/2$ reference CSF, it is enough to give the two sets of data: [4s, 4p] and [4p, 4d, 4f] and all CSF with $J = 3/2$ will be build automatically. Note that input data for the orbitals are given in LS coupling but all associated jj subconfigurations are generated internally.

- The so-called optimized levels (OL) method was used for each state considered. This allow for a full relaxation of the initial and final states and provide much better energies and wave functions. However, in this method, one-electron orbitals in the initial and final states are not orthogonal. The formalism to take into account the non-orthogonality in the transition probabilities calculation has been described by Löwdin [11] and Slater [12]. The matrix element of a one-electron operator O between two determinants belonging respectively to the initial and final states can be written as

$$\sum_{ij} \langle \phi_i | O | \phi'_j \rangle \xi_{ij} D^1_{ij}, \tag{10}$$

where the ϕ are the initial state orbitals and the ϕ' the final state ones. D^1_{ij} is the first order cofactor obtained by crossing out the ith row and jth column from the $n \times n$, overlaps' matrix, and $\xi_{ij'} = \pm 1$ the associated phase factor. In the code, after building the overlap matrix, cofactors are calculated using standard LU decomposition.

3. The $^4D_{7/2}$ KrII metastable level

The single ionized Krypton ion is used to check the minimum of correlation to include in order to reach a reasonable agreement with experimental results. Fig. 1 below displays the main available decay channels, as none is an electric $E1$ this a strong evidence for the metastability of this level. For the Dirac–Fock optimum level approximation (i.e., including full relaxation between the initial and final states) and with only the Coulomb interaction in the SCF process, the results are given in Table 1 (length gauge values for the electric transitions). As the

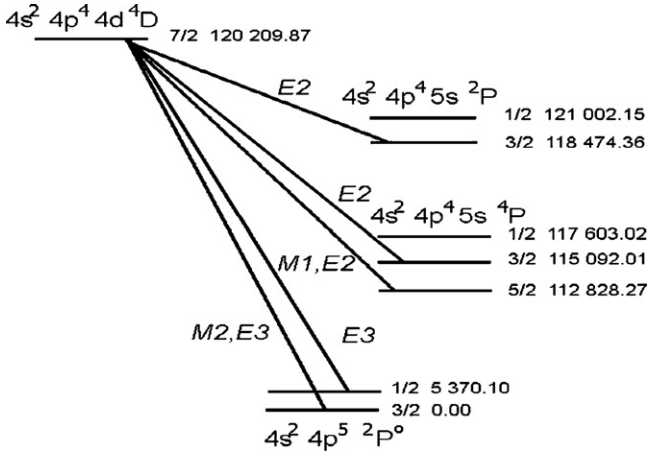

Fig. 1. Main decay channels for the^{4}D7/2level of KrII (the experimental energies, in cm^{-1}, are taken from [13]).

Table 1
Dirac–Fock decay rates, using experimental energies, for the $^4D_{7/2}$ level of KrII

Final configuration	Level	Channel	Rate [a] (s^{-1})
$4s^2 4p^4_{3/2} 5s$	$^2P_{3/2}$	$E2$	4.61(−6)
	$^4P_{3/2}$	$E2$	2.80(−3)
	$^4P_{5/2}$	$M1$	6.33(−12)
		$E2$	7.03(−2)
$4s^2 4p^5_{3/2}$	$^2P^o_{1/2}$	$E3$	1.52(−5)
	$^2P^o_{3/2}$	$M2$	1.01
		$E3$	3.24(−5)

[a] $a(b)$ stands for $a \times 10^b$.

channels considered are of various multipolarities with strong different energy scaling, we start by using experimental transition energies to avoid bias in selecting the relevant contributions. We shall discuss this point more deeply when analyzing the influence of correlation. According to these Dirac–Fock results, the dominant decay channel for the $^4D_{7/2}$ level is the $M2$ transition to the $^2P^o_{3/2}$ ground state, in agreement with the conclusion of [1]. We shall nevertheless point out that the present rate is about four times greater than the one reported in [1](0.28 s^{-1}), this cannot be explained by the use of the experimental energy, indeed as their theoretical value is greater than experiment, the E^5_T scaling of the $M2$ transition probability with the transition energy E_T would have resulted is a still lower rate should the experimental value has been used. This show the importance of relaxation in the orbitals between the initial and final states as included in the OL calculations as opposed to the optimization of the wave functions for a weighted sum of initial and final states as done in [1].

From now on we include the magnetic part of the Breit interaction (Eq. 4) in the self-consistent field process but restrict our discussion of the correlation effects on the strong $M2$transition. We may expect that the most important correlation effects will arise from the the intra-shell contribution within the $n = 4$ valence shell. We begin by restricting the subspace to the 4s, 4p and 4d occupied orbitals in the excited level, then we add the $4f$ orbital. For these two sets of calculations all single and double excitations from the Dirac–Fock reference state are included. Again let us recall that amounts to take care of excitations from the four jj subconfigurations $4p^2_{1/2}4p^2_{3/2}4d_{3/2}$, $4p_{1/2}4p^3_{3/2}4d_{3/2}$, $4p^2_{1/2}4p^2_{3/2}4d_{5/2}$ and $4p_{1/2}4p^3_{3/2}4d_{5/2}$ of the $^4D_{7/2}$ excited level. The $^2P_{3/2}$ ground state is much simpler because of its single $4p^2_{1/2}4p^3_{3/2}$ jj configuration. To extend the basis, a third calculation includes all jj subconfigurations arising from the two LS configurations $4p^4 5d$ and $4p^4 5g$ for the excited level and the $4p^4 5p$ and $4p^4 5f$ for the ground level.

The agreement with experiment, of the results in the last line of Table 2, is within about 2% for the transition energy and 25% for the lifetimes ($\tau = 1/1.401 = 0.714$ s to be compared to $\tau = 0.57 \pm 0.03$ s as reported in [1]). To analyze the contribution of correlation to the transition rate it is worth separate it into two contributions: first the change induced in the transition energy and, second, the one resulting from the extension in the number of configuration state functions (that include also modifications

Table 2
Influence of correlation on the $M2$ decay channel of the $^4D_{7/2}$ level of KrII (using theoretical energy)

Approximation	Energy (cm^{-1})	Rate (s^{-1})
Dirac–Fock	113,582	0.757
1 and 2 electron excitations up to 4d	123,791	1.432
1 and 2 electron excitations up to 4f	123,492	1.468
Above plus $n = 5$ configurations	122,743	1.401

in the orbital radial functions). To get the second contribution one has simply to rescale the rates to a common transition E_T. Using the energy of the fourth line, the Dirac–Fock rates becomes 1.116 s^{-1}showing that the change in the transition energy is by far the most important contribution.

To conclude this section let us considered also the small contributions of the other decay channels when including the same amount of correlation, Table 3 displays these results.

The agreement between the length and velocity forms for the electric decay channels to the various levels of the $4s^24p^45s$ configuration is poorer than those to the $4s^24p^5$ configuration, an indication that more correlation needs to be included. Nevertheless as these contributions are at the few percent level (the lifetimes of 0.714 s^{-1} of the single M 2 decay channel being change to 0.696/0.707 s^{-1}) it is not worth trying to improve for the purpose of this paper. Even if, in the relativistic case, the gauge independence cannot be achieved without including the negative energy states [14], it is unlikely that their contribution will be significant for the valence electrons considered here. Known from a long time [15], but explained only recently [16], relativistic LSJ levels will not always reduced to the same LS level in the formal limit of the speed of light going to infinity, thus leading to a potential bias in the fine structure splittings. For the present calculations this is a negligible contribution in the error of the transition energies since the offset in the LS levels is 13 $cm^{-1}$for the $4s^24p^5$ configuration and 15 cm^{-1} for the $4s^24p^44d$ one.

4. Trends along the iso-electronic sequence

Instead of the single $4p^44d$ LS configuration, the $^4D_{7/2}$ level involves, in jj coupling, the four subconfigurations $4p^2_{1/2}4p^2_{3/2}4d_{3/2}$, $4p^2_{1/2}4p^2_{3/2}4d_{5/2}$, $4p_{1/2}4p^3_{3/2}4d_{3/2}$ and $4p_{1/2}4p^3_{3/2}4d_{5/2}$ whose contributions in the non relativistic limit are respectively 4.4%, 2.2%, 40% and 53.4%, summing in the last value the contributions of the two degenerated $4p_{1/2}4p^3_{3/2}4d_{5/2}$ subconfigurations. A small departure from these percentages is already observed for the neutral Bromine. When the atomic number Z increases, the weight of the subconfiguration $4p^2_{1/2}4p^2_{3/2}4d_{3/2}$ that maximize the occupation of the $j = l - 1/2$ orbitals will increase to become almost the only meaningfull contribution at high Z as illustrated in Fig. 2, this behavior is the result of the strong spin-orbit interaction.

Table 3
MCDF decay rates, using theoretical energies, for the $^4D_{7/2}$ level of KrII

Final configuration	Level	Energy (cm^{-1})	Channel	Rate [a] (s^{-1})
$4s^24p^4_{3/2}5s$	$^2P_{3/2}$	3934	$E2$	1.24(−3)/2.60(−3)
	$^4P_{3/2}$	3997	$E2$	1.35(−3)/2.78(−3)
	$^4P_{5/2}$	6577	$M1$	5.27(−5)
			$E2$	3.16(−2)/7.84(−3)
$4s^24p^5_{3/2}$	$^2P^o_{1/2}$	117,467	$E3$	1.73(−4)/1.91(−4)
	$^2P^o_{3/2}$	122,743	$M2$	1.40
			$E3$	1.31(−3)/1.48(−3)

[a] $a(b)$ stands for $a \times 10^b$ and the two values for the electric decay channels are respectively the length and velocity values.

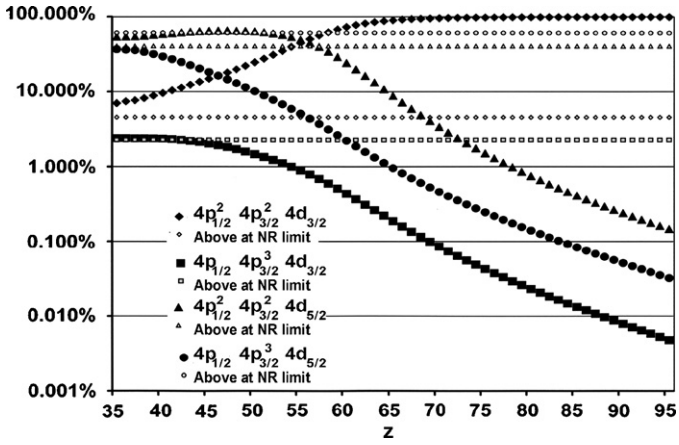

Fig. 2. Weights of the jj subconfigurations in the lowest $J = 7/2$ level of the $4p^44d$ configuration. Straight lines labeled with NR limit are the values for the pure $^4D_{7/2}$ LSJ term.

For relativistic calculations the only angular momentum commuting with the Hamiltonian is the total J. Consequently, even at the Dirac–Fock approximation, any $J = 7/2$ level will include mixing between the five LSJ terms $^2F_{7/2}$, $^4F_{7/2}$, $^4D_{7/2}$ (from $4p^4(^3P)4d$) and $^2G_{7/2}$, $^2F_{7/2}$ (from $4p^4(^1D)4d$). As display in Fig. 2, the lowest term $^4D_{7/2}$ at the beginning of the sequence include only a small contribution from the jj $4p^2_{1/2}4p^2_{3/2}4d_{3/2}$ subconfiguration that is becoming dominant at high Z, thus a drastic change in the LSJ term contributions to the lowest $J = 7/2$ level along the sequence can be expected. Indeed, for the lowest level, the $^4D_{7/2}$ term is no more the dominant contribution beyond $Z \geq 60$ and for $Z = 95$ we obtain percentages of 29%, 29%, 36% and only 6% for respectively the $^2G_{7/2}$, $^4F_{7/2}$, $^2F_{7/2}$, $^4D_{7/2}$ terms as shown in Fig. 3. As the code computes the eigenstates of J^2 by a matrix diagonalization of all $M_J = 7/2$ determinants without intermediate recoupling of individual shells, we cannot assign the $^2F_{7/2}$ terms to one of the two $4p^4(^3P)4d$ or $4p^4(^1D)4d$ recouplings, this is why they are just labeled 1 and 2 in Fig. 3.

From the analysis of correlation effects for KrII in the previous section we are able to select the minimum of correlation to include along the Bromine sequence to get reasonable estimates of lifetimes. First, the $E2$ weak decay channels to the $4p^45s$ levels have not to be included since they are no more available beyond $Z = 36$. In agreement with the experimental tables of energy levels [13], the Dirac–Fock calculations show that the $4p^45s$ levels are above those of the $4p^44d$ configuration starting from RbIII. Next, the increase in the splitting between the $n = 4$ and $n = 5$ atomic orbitals with Z will decrease the coupling with excitations to the $n = 5$ orbitals and as their con-

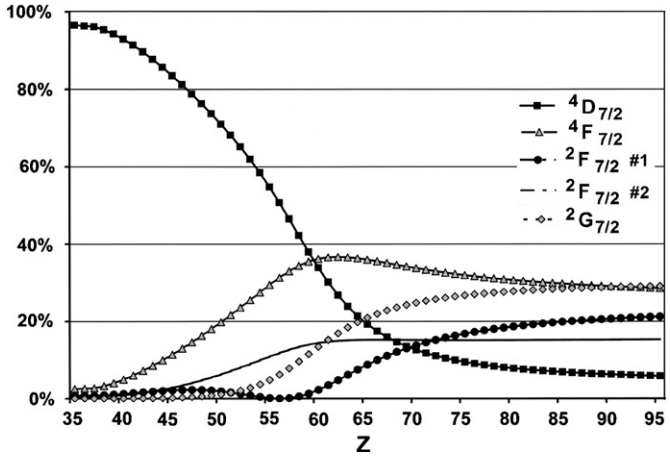

Fig. 3. Contributions of the LSJ terms to the lowest $J = 7/2$ level of the $4p^4 4d$ configuration.

tribution is already small (see Table 3) we can also safely ignored them. Last, the $E3$ decay channel to the $4p^5\ ^2P^o_{1/2}$ state remains weak before disappearing at $Z = 85$ because the energy of this level becomes higher than the lowest $J = 7/2$ one of the excited $4p^4 4d$ configuration. This may appear surprising but should have been expected from the j degeneracy of the hydrogenic Dirac energies for the $4p_{3/2}$ and $4d_{3/2}$ orbitals and the large spin-orbit splitting (greater than 150 eV for Bromine ions with $Z > 80$). Nevertheless the decrease in the transition probability is so sharp (5 orders of magnitude between $Z = 80$ and $Z = 84$) that we think worth to illustrate it in Fig. 4.

Retaining only the $n = 4$ intra-shell correlations, the rates from the lowest $J = 7/2$ are plotted in Fig. 5. For the $M2$ channel, one observes that, instead of a monotonous increasing behavior with Z, the rate starts to increase up to a maximum around $Z = 55$ and then decreases to recover almost the near neutral limit. Correlation effects saturate to about 10% at the end of the sequence, a difference overwhelmed between the two curves labeled *DF* and *Correl.* because of the logarithmic scale. More visible is the fact that correlations increase the rate at low Z but decrease it at high Z. If the $E3$ channel remains weak almost all the long of the sequence, it nevertheless becomes the dominant channel at very high Z values.

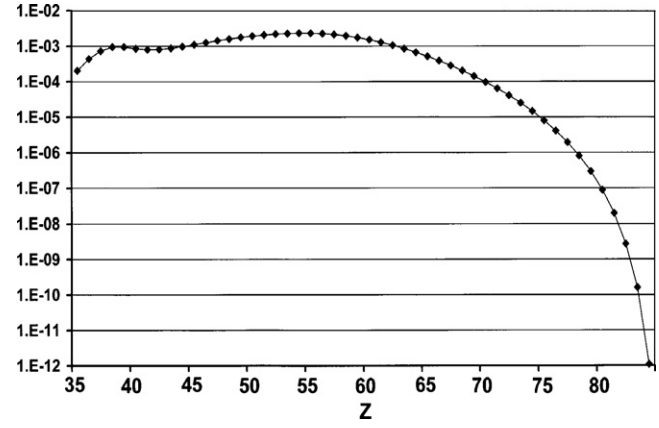

Fig. 4. Electric $E3$ rate (in s^{-1}) to the $4p^5 {}^2P^o_{1/2}$level.

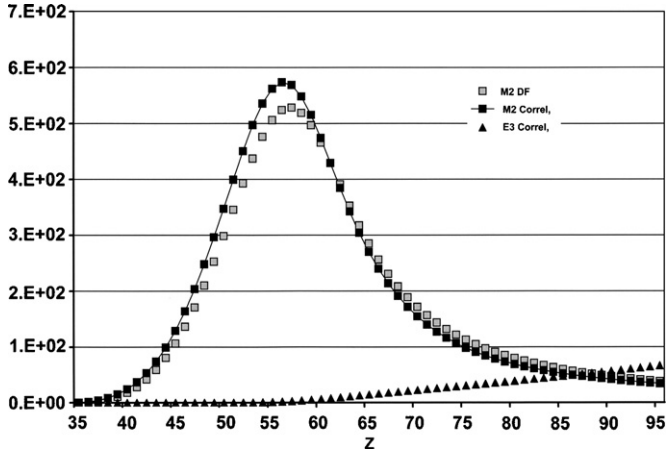

Fig. 5. Rates (in s^{-1}) of the lowest $4p^4 4d$ $J = 7/2$ level.

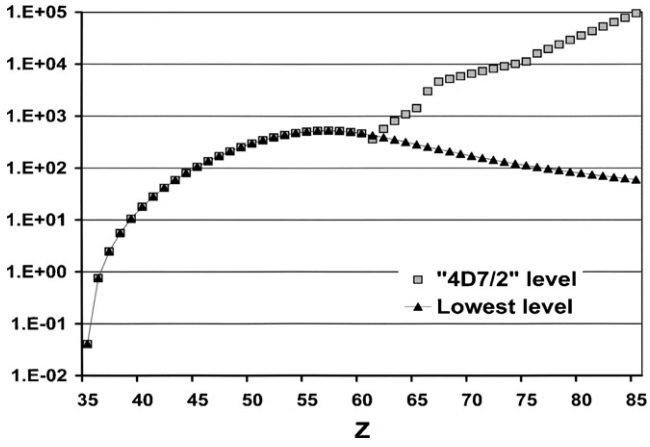

Fig. 6. Comparison of the lowest $J = 7/2$ and "$^4D_{7/2}$" levels Dirac–Fock rates (in s^{-1}).

The maximum for the $M2$ rate in Fig. 5 arises almost at the same Z value for which the $^4D_{7/2}$ term is no more the largest contribution to the lowest $J = 7/2$ level (see Fig. 3). To confirm that the transition from LSJ to *jj* coupling is the source of the $M2$ rate behavior we use the option of the code to seek convergence to the level having the largest contribution from a given LSJ term. In so doing we obtain the results display in Fig. 6 that unambiguously show that the behavior of the rate from the level with maximum $^4D_{7/2}$ term contribution departs strongly from the rate of the lowest $J = 7/2$ beyond $Z = 60$. This rate is continuously increasing and reaches a value of 6.6×10^5 at $Z = 95$ even if the weight of the $^4D_{7/2}$ term is only about 4/9 with a strong mixing with the $^4F_{7/2}$ term.

5. Conclusions

The results of the previous sections show that the multiconfiguration Dirac–Fock method (MCDF) is well adapted to take care of the intra-shell correlation effects even with a large underlying core. These intra-shell contributions are the first one to include to reach meaningfull theoretical results to compare with experiment. Obviously correlation between core and valence electrons is missing from these calculations but the MCDF approach will

be quite inefficient with a 28-electron core. Furthermore, even if saturating the power of modern computers, it will be very difficult to maintain balanced contributions between the two levels involved in the transitions. As said in the introduction our aim was to seek the minimum of sophistication to produce physically relevant results and not to achieve the most accurate possible ones. Using a limited set of configuration state configurations (CSF) the contribution of orbital relaxation between initial and final states can be easily included and was show to be important, neglecting it will need to include a much larger number of CSF to recover its contribution. Besides correlation effects, the transition from LSJ to *jj* couplings was investigated with the conclusion that trends along an iso-electronic sequence cannot be extrapolated from behaviors at low *Z* values. The impact of large spin-orbit splittings at very high *Z* should not be underestimated in the ordering of energy levels between different configurations. With respect to these last two comments, Fig. 6 and 4 are the most illustrative. All the calculations were done on a PC, taking about two minutes of CPU time per ion, using the Linux OpenSuse operating system and the Intel Fortran compiler.

Acknowledgements

Late Y.K. Kim raised up my interest for iso-electronic sequences at an early stage of our collaboration that held out without interruption for 35 years. Computers from that times had very modest power with respect to nowadays standards, Yong-Ki taught the young physicist, me, how to think about physics before rushing to punch input data cards. Many options in the *mdfgme* code were implanted at his suggestions to explore relativistic effects in atomic structure. Paul Indelicato is gratefully acknowledged for numerous contributions to the code, in fact he implemented most of the extensions for the radiative decay rates used in the present work. Thanks also to him for a critical reading of the manuscript.

References

[1] E. Biémont, A. Derkatch, P. Lundin, S. Mannervik, L.-O. Norlin, D. Rostohar, P. Royen, P. Palmeri, P. Schef, Phys. Rev. Lett. 93 (2004), 063003-1.
[2] J. Desclaux, P. Indelicato, MDFGME: a multi-configuration Dirac–Fock and general matrix elements program (release 2005), http://dirac.spectro.jussieu.fr/mcdf.
[3] J.P. Desclaux, Comp. Phys. Commun. 9 (1975) 31.
[4] J.P. Desclaux, in: E. Clementi (Ed.), Methods and Techniques in Computational Chemistry, vol. A: Small Systems STEF, Cagliary, 1993.
[5] P. Indelicato, Phys. Rev. A 51 (1995) 1132.
[6] P. Indelicato, Phys. Rev. Lett. 77 (1996) 3323.
[7] O. Gorceix, P. Indelicato, Phys. Rev. A 37 (1988) 1087.
[8] E. Lindroth, A.M. Mårtensson-Pendrill, Phys. Rev. A 39 (1989) 3794.
[9] P. Indelicato, J.P. Santos, S. Boucard, J.-P. Desclaux, Eur. Phys. J. D 45 (2007) 155.
[10] I. Angeli, At. Data Nucl. Data Tables 87 (2004) 185.
[11] P.O. Löwdin, Phys. Rev. 97 (1955) 1474.
[12] J.C. Slater, Quantum Theory of Molecules and Solids, vol. 1 of International Series in Pure and Applied Physics, McGraw-Hill, New York, 1963.
[13] NIST Atomic Spectra Database Levels Data, http://physics.nist.gov/PhysRefData/ASD/.
[14] U.I. Safronova, W.R. Johnson, H.G. Berry, Phys. Rev. A 61 (2000) 052503.
[15] K.N. Huang, Y.K. Kim, K.T. Cheng, J.P. Desclaux, Phys. Rev. A 48 (1982) 1245.
[16] P. Indelicato, E. Lindroth, J.P. Desclaux, Phys. Rev. Lett. 94 (2005) 013002.